34th Annual International Conference of the IEEE EMBS
San Diego, California USA, 28 August - 1 September, 2012

Estimating Electrical Conductivity Tensors of Biological Tissues Using Microelectrode Arrays

Elad Gilboa[1], Patricio S. La Rosa[2], and Arye Nehorai[3]

Abstract— **Finding the electrical conductivity of tissue is important for understanding the tissue's structure and functioning. However, the inverse problem of inferring spatial conductivity from data is highly ill-posed and computationally intensive. In this paper, we propose a novel method to solve the inverse problem of inferring tissue conductivity from a set of transmembrane potential and stimuli measurements made by microelectrode arrays (MEA). We propose a parallel optimization algorithm based on a single-step approximation with a parallel alternating optimization routine. This algorithm simplifies the joint tensor field estimation problem into a set of computationally tractable subproblems, allowing the use of efficient standard optimization tools.**

I. Introduction

Transmembrane potential propagation in biological tissue results when the ionic concentrations change in either the intracellular or extracellular domains. Potential propagation is correlated with the medium's conductivity, and as a mechanism of intercellular communication it plays an important role in tissue and organ functioning [1]. A classical approach to modeling spatiotemporal transmembrane potential propagation is based on the generalized cable theory, combined with dynamic models of ionic concentration gradients. The bidomain model treats the tissue as two continuous domains, and is a macroscale model of the electrical behavior averaged over many cells, taking into account both the intracellular and extracellular current flows. Although this model has been used extensively in numerical simulations of the electrical behavior of anisotropic myocardiac tissues [2], in neuroscience it has recently been used for analyzing the non-homogeneity of the extracellular domain in nerve tissues [3].

In the last few years, much progress has been made in developing high-resolution microelectrode arrays (MEA) that allow electrophysiological measurements of biological tissues with high spatiotemporal resolution [4]. Using this technology, it is possible to effectively and directly measure transmembrane potential propagation by parallel measurements of the tissue at different locations. By employing the biodomain model to analyze the MEA data, we gain a deeper understanding of the underlying biophysical nature of tissue.

This work was supported in part by the McDonnell International Scholars Academy Fellowship, and also in part by a National Science found CCF-0963742.

[1]E. Gilboa (gilboae@ese.wustl.edu) and [3]A. Nehorai (nehorai@ese.wustl.edu) are with the Preston M. Green Department of Electrical and Systems Engineering, Washington University in St. Louis, St. Louis, MO 63130.

[2]P.S. La Rosa (PLAROSA@DOM.wustl.edu) is with the Department of Medicine-Division of General Medical Sciences, Washington University in St. Louis, School of Medicine, St. Louis, MO 63110.

In this work, we develop a mathematical framework for solving the inverse problem of estimating the effective electrical tissue conductivities from a set of electric potentials and stimulus measurements. In particular, we formulate the problem in a system identification framework, using a parametric model based on the generalized cable theory. In this framework, experiments are performed by exciting the system and observing its input/output over a time interval. Unfortunately, solving this ill-posed inverse problem is highly complex. Specifically, it suffers from *high dimensionality* (as one must estimate the tensor matrix for each point in space), *nonlinearity* (due to the nonlinear extracellular field potential dynamics), and *stochasticity* (as the observations are corrupted by noise).

This paper makes two contributions. First, we introduce a discrete forward model of transmembrane potential based on a diffusion-reaction model with an anisotropic inhomogeneous electrical conductivity-tensor field. Second, we propose a novel parallel optimization algorithm for solving the complex inverse problem of estimating the conductivity tensor field.

II. Forward Model

To model electrical propagation in biological tissue, we use the generalized cable approach, namely, the monodomain approach [5]. In the monodomain model, biological tissue is reduced to a two- or three-dimensional cell grid, where the electrical behavior is governed by a set of reaction-diffusion equations. The diffusion part of this model represents the spatial evolution of the transmembrane potential in a domain with changing conductivities. The reaction part models the voltage-dependent dynamics of the cells. Our system can be written as follows:

$$\underbrace{\boldsymbol{\nabla}\cdot\boldsymbol{D}(\boldsymbol{r})\boldsymbol{\nabla}v(\boldsymbol{r},t)}_{\text{Diffusion}} = \underbrace{a_{\mathrm{m}}\left(c_{\mathrm{m}}\frac{\partial v(\boldsymbol{r},t)}{\partial t}+\mathrm{j}_{\mathrm{ion}}(v(\boldsymbol{r},t),\boldsymbol{w},\boldsymbol{\phi},t)-\mathrm{j}_{\mathrm{stim}}(\boldsymbol{r},t)\right)}_{\text{Reaction}}, \tag{1}$$

$$v(\boldsymbol{r},0)=v_0, \tag{2}$$

$$\boldsymbol{\nabla}v(\boldsymbol{r},t)\cdot\boldsymbol{n}(\boldsymbol{r})=0, \boldsymbol{r}\in\partial C, \tag{3}$$

where $t\in[0,T]$, the spatial vector $\boldsymbol{r}$ belongs to $C\subseteq\mathbb{R}^p$, the domain C is a bounded Euclidean subset, $\boldsymbol{n}$ denotes the normal to the boundary, and ∂C is the boundary of domain C. In this work we consider the 2D case, where $p=2$. Furthermore, $\mathrm{j}_{\mathrm{stim}}(\boldsymbol{r},t)$ is the stimulus volume

current density ($\mathrm{A/m^3}$); c_m is the membrane capacitance per unit area ($\mathrm{F/m^2}$); a_m is the surface-to-volume ratio of the membrane ($1/\mathrm{m}$); and $\boldsymbol{D}(\boldsymbol{r}) \in \mathbb{S}_{2++}$ is the positive definite conductivity tensor. $\mathrm{j_{ion}}(v(\boldsymbol{r},t), \boldsymbol{w}, \boldsymbol{\phi}, t)$ is the ionic volume current density ($\mathrm{A/m^3}$) of a biological cell, and it can be chosen to fit a specific dynamic, with $\boldsymbol{w}$ corresponding to the internal state vector, and $\boldsymbol{\phi}$ to the model parameters. For simplicity, we consider a homogenous cell dynamic in the tissue; namely, $\boldsymbol{\phi}$ is consistent in all the cells (in the results section, we used the extended FitzHugh-Nagumo (FHN) equations [6] as a fairly general and simple representation of a cell's ionic currents; however, more extensive models can be used). Eqs. (2) and (3) present the initial temporal and boundary conditions, respectively. In particular, we use the homogenous Neumann boundary condition since we assume that there will be no current through the borders of the domain, and we use the *zero state response* for the initial values since we assume that the system is initially relaxed at its resting potential v_0 and cannot initiate a spontaneous response.

A. Modeling Tissue Anisotropy

In order to infer the underlying conductivity structure of the tissue, we represent biological tissue as a continuous field of conductivity tensors, $\boldsymbol{D}(\boldsymbol{r})$ in Eq. (1), which models local extracellular conductivities within the tissue [5]. To simplify the problem, we consider working with only a thin slice of tissue that can be represented as a 2D plane. The conductivity tensor is given by

$$\boldsymbol{D}(x,y) = \begin{bmatrix} \sigma_\mathrm{x}(x,y) & \sigma_\mathrm{xy}(x,y) \\ \sigma_\mathrm{xy}(x,y) & \sigma_\mathrm{y}(x,y) \end{bmatrix}, \tag{4}$$

where $\sigma_\mathrm{x}(x,y), \sigma_\mathrm{xy}(x,y), \sigma_\mathrm{y}(x,y)$ are the conductivity values in the horizontal, diagonal, and vertical directions, respectively. The tensor field is an indexed set of tensors in space, and is referred to as *isotropic* if all the conductivity tensors are directionally independent (symmetric), that is, $\sigma_\mathrm{x}(x,y) = \sigma_\mathrm{y}(x,y) = \sigma_0$ and $\sigma_\mathrm{xy}(x,y) = 0$ for all x, y. Otherwise, if some conductivity tensors in the field are directionally dependent, it is referred to as *anisotropic*. If the conductivity tensors are constant throughout the field, then the field is referred to as *homogeneous*; otherwise, it is *inhomogeneous*. A diffusion tensor can be expressed in terms of its eigenvalues $\boldsymbol{\lambda} = (\lambda_1, \lambda_2, \lambda_3)$ and eigenvectors $\boldsymbol{E} = (\boldsymbol{e}_1, \boldsymbol{e}_2, \boldsymbol{e}_3)$ as $\boldsymbol{D} = \boldsymbol{E}^T \mathrm{diag}(\boldsymbol{\lambda}) \boldsymbol{E}$. The tensor can be represented as an ellipsoid, whose radii (eigenvalues) represent the amount of diffusion (flow) in each of the main directions (eigenvectors).

B. Discretization

To transfer our model from a continuous domain into a discrete vector space formulation, we will to discretize the continuous diffusion term of Eq. (1), using the Finite-Difference Method (FDM) with an forward-time central-space scheme to approximate the derivatives, taking into account the spatially varying tensor field of Eq. (1). In practice we observe $\boldsymbol{v}_n$ through spatiotemporal measurements $\boldsymbol{y}_n \in \mathbb{R}^Q$. Here we will assume that $\boldsymbol{y}_n$ are corrupted with an additive white Gaussian noise of mean zero and variance γ^2. Therefore, the discretized system and measurements model is given by

$$\boldsymbol{v}_{n+1} = \mathbf{f}(\boldsymbol{v}_{0:n}, \boldsymbol{w}_{0:n}, \boldsymbol{\phi}, \boldsymbol{\Theta}) + b\boldsymbol{u}_n, \tag{5}$$

$$\boldsymbol{y}_n = \boldsymbol{v}_n + \boldsymbol{\nu}, \tag{6}$$

where $\boldsymbol{\Theta} = \{\boldsymbol{\Theta}_1, \boldsymbol{\Theta}_2, \ldots, \boldsymbol{\Theta}_K\}$ is a joint set of K tensors of the form $\boldsymbol{\Theta}_k = \begin{bmatrix} \sigma_{\mathrm{x}k} & \sigma_{\mathrm{xy}k} \\ \sigma_{\mathrm{xy}k} & \sigma_{\mathrm{y}k} \end{bmatrix}$ at location k. We will refer to this set $\boldsymbol{\Theta}$ as the discrete conductivity-tensor field.

III. Solving the Inverse Problem

The goal of solving the inverse problem is to estimate $\boldsymbol{\Theta}$, the discretized tensor field of tissue conductivity, from the set of measurements $\boldsymbol{y}_{0:T}$, the set of inputs $\boldsymbol{u}_{0:T}$, and the discrete system model in Eqs. (5) (6). Here we use an indirect method to estimate $\boldsymbol{\Theta}$, by transferring it into an optimization problem. There are several methods in the literature to solve this inverse problem, such as the augmented Lagrangian method [7], Initial Value Approach (IVA) [8], and the patched unscented Kalman filter (PUCF) [9]. However, these methods may not suffice as the augmented Lagrangian method is highly computationally intensive, the IVA is very sensitive to initial conditions, and the PUCF lowers the resolution substantially. As a result, in order to solve this complex multidimensional inverse problem, we propose a simpler, nonrecurrent method based on the ideas of one-step prediction and alternating optimization.

A. One-Step Prediction (OSP)

When dealing with invasive electrophysiological recordings, it is acceptable to assume low sensor measurement noise and use the observed data as a direct measurement of the average local field potential states, $\boldsymbol{y}_n \approx \boldsymbol{v}_n$ [10]. By using the observations instead of the states, we can write the discrete system model as

$$\hat{\boldsymbol{y}}_{n+1} = \mathbf{f}(\boldsymbol{y}_n, \boldsymbol{w}_n, \boldsymbol{\phi}, \boldsymbol{\Theta}) + b\boldsymbol{u}_n. \tag{7}$$

To then write the OSP score function we use the LS between the one-step predictions and the measurements, which is given by

$$\mathrm{V_{OSP}}\left(\boldsymbol{y}_{0:N}, \boldsymbol{w}_0, \boldsymbol{u}_{0:N}, \boldsymbol{\phi}, \boldsymbol{\Theta}\right) = \sum_{n=1}^{N} \sum_{k=1}^{K} \left(\boldsymbol{y}_{n,k} - \mathbf{f}\left(\boldsymbol{y}_{n-1}, \boldsymbol{w}_0, \boldsymbol{\phi}, \boldsymbol{\Theta}\right)_{n,k} - b\boldsymbol{u}_{n,k} \right)^2. \tag{8}$$

B. Parallel Alternating Optimization

In the alternating optimization class of algorithms, a complex optimization problem is solved by iteratively solving a series of easy to handle subproblems. The algorithm then iteratively cycles through the different subproblems and updates the parameters in each subset until convergence is reached. However, even for a modest size grid, the high-dimensionality of the problem will make the alternating optimization problem computational expensive as it will have

to sequentially alternate between many parameter subspaces. To improve computational costs, we vary the alternate optimization algorithm so that instead of sequentially solving the set of subproblems, we solve them in parallel and join them after each iteration.

The K optimization routines can be written as

$$\hat{\boldsymbol{\Theta}}_k^{[j]} \leftarrow \arg\min_{\substack{\boldsymbol{\Theta}_k=\{\sigma_{\mathrm{x}k},\sigma_{\mathrm{xy}k},\sigma_{\mathrm{y}k}\} \\ \boldsymbol{\Theta}_k\in\mathbb{S}_{2++}}} \tag{9}$$

$$\mathrm{V}_{\mathrm{OSP}}\left(\boldsymbol{y}_{0:N}, \boldsymbol{w}_0, \boldsymbol{u}_{0:N}, \boldsymbol{\phi}, \hat{\boldsymbol{\Theta}}_{i\neq k}^{[j-1]}, \boldsymbol{\Theta}_k\right) + \lambda \mathrm{d}\left(\boldsymbol{\Theta}_k, \hat{\boldsymbol{\Theta}}_k^{[j-1]}\right),$$

where λ is the Lagrangian hyper-parameter. The step-size penalty feature is added to the algorithm to reduce the probability of the algorithm becoming stuck at a local minimum that is worse than the global one. The joint parameter set at iteration j, $\hat{\boldsymbol{\Theta}}^{[j]}$, is simply the union of the solutions to the K optimization problems.

Finally, we use these ideas to write a parallel OSP algorithm (pOSP) which iterates between parallel estimation of conductivity tensors and estimation of the initial internal states $\boldsymbol{w}_0$. The full iterative pOSP algorithm is presented in Alg. 1. [1]

Algorithm 1 Parallel OSP

procedure pOSP($\boldsymbol{\Theta}^0, \boldsymbol{w}_0^0$) ▷ $\boldsymbol{\Theta}^0 \in \mathbb{S}_{2++}, w_0^0 \in \mathbb{R}$
  $\boldsymbol{\Theta}_{\forall k\in K}^0 \leftarrow \boldsymbol{\Theta}^0$
  $\boldsymbol{w}_0^0 \leftarrow w_0^0\mathbf{1}$
  $j \leftarrow 0$
  repeat
    $j \leftarrow j+1$
    parfor $k \in K$ **do**
    $\hat{\boldsymbol{\Theta}}_k^{[j]} \leftarrow \arg\min_{\boldsymbol{\Theta}_k\in\mathbb{S}_{2++}}$
      $\mathrm{V}_{\mathrm{OSP}}\left(\boldsymbol{\Theta}_k, \hat{\boldsymbol{\Theta}}_{i\neq k}^{[j-1]}, \boldsymbol{w}_0^{[j-1]}, \boldsymbol{y}\right)$
      $+ \lambda \mathrm{d}\left(\boldsymbol{\Theta}_k, \hat{\boldsymbol{\Theta}}_k^{[j-1]}\right) + \mathrm{h}\left(\boldsymbol{\Theta}_k, \hat{\boldsymbol{\Theta}}^{[j-1]}\right)$
    end parfor
    $\hat{w}_0^{[j]} \leftarrow \arg\min_{w_0\in\mathbb{R}} V(\boldsymbol{\Theta}^{[j]}, w_0, \boldsymbol{y})$
    $\boldsymbol{w}_0^{[j]} \leftarrow \hat{w}_0^{[j]}\mathbf{1}$
  until convergence
  return
end procedure

The last term of the $\arg\min$ is an optional spatial penalization function $\mathrm{h}\left(\boldsymbol{\Theta}_k, \hat{\boldsymbol{\Theta}}^{[j-1]}\right)$, which penalizes large spatial deviations from *a priori* information of the tissue. Prior information can be provided from other sources, such as anatomical data, or from biological knowledge of the tissue properties, such as smoothness in smooth muscle tissues. For the spatial penalization function, we choose the following form:

$$\mathrm{h}\left(\boldsymbol{\Theta}_k, \hat{\boldsymbol{\Theta}}^{[j-1]}\right) = \sum_{k=1}^{K} \mu\left(\boldsymbol{L}_{xy}^2\boldsymbol{\sigma}_{\mathrm{x}} + \boldsymbol{L}_{xy}^2\boldsymbol{\sigma}_{\mathrm{xy}} + \boldsymbol{L}_{xy}^2\boldsymbol{\sigma}_{\mathrm{y}}\right), \tag{10}$$

[1]Minimization performed using a standard Matlab implementation of the sequential quadratic programming method.

where $\boldsymbol{L}_{xy}^2$ is the $2D$ discrete Laplace operator, and μ is the penalty weight.

IV. Results

To analyze the performance of the pOSP algorithm, we compiled a number of test simulations to examine the algorithm's ability to estimate the tensor field of different field topologies under varying noise levels. For a fairly general and simple representation of a cell's ionic current dynamics, we use extended FitzHugh-Nagumo (FHN) equations. The values of the reaction parameters for the simulations were fitted to a slow wave from a pregnant human's uterine myocyte, as presented in [5].

A. Step-Size Penalty λ

The hyper-parameter λ, which was introduced in the previous section, is the weight of the penalty term we added in order to control the step size of the pOSP algorithm. In this work we used $\lambda = 10^{-4}$, which might be suboptimal for different problems.

To test the significance of the step-size penalty on the optimization algorithm, we compared the standard sequential alternating optimization to the parallel alternating optimization, with and without a step-size penalty ($\lambda = 10^{-4}$), for various noise levels. We compared both the accuracy and the computational time for the algorithms, using ten iterations on a toy 8×8 Gaussian mixture. From Fig. 1, we can observe that the parallel alternating optimization algorithm with a step-size penalty (PAOSS) achieves considerably better estimation results than the one without a step-size penalty. Furthermore, for all tested noise levels, the PAOSS estimation offers estimation accuracy comparable to that of the standard alternating optimization algorithm, at a significantly lower computation time.

B. Richness of Inputs

A fundamental factor in the algorithm's ability to correctly identify the spatially varying conductivity-tensor field is the choice of input signals used to excite the system. The input must possess sufficient richness in both its spatial and temporal excitations to guarantee enough spatiotemporal information to fully identify the system. For our simulations, we considered three types of spatially varying tensor fields: constant, Gaussian mix, and circular. To test the improvement of the pOSP conductivity-tensor estimation, we tested the algorithm with different numbers of stimulations. The simulations were sequential, with 150 time-steps between each simulation. In Fig. 2, we present the resulting log mean squared error between the estimated conductivity tensor field and the original real field for the three fields, where the estimated field is considered as a function of the number of simulations. As the number of stimulations increased, the MSE monotonically decreased toward zero. Greatest improvement was achieved when the spatial location of the new stimulus was significantly different from the previous stimuli with respect to the field topology. In the Gaussian case, an increase in MSE can be observed as a result

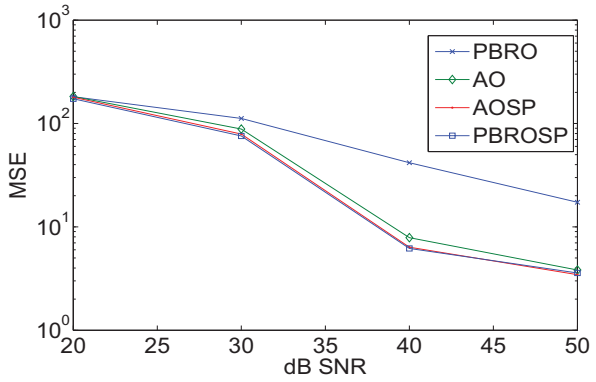

(a)

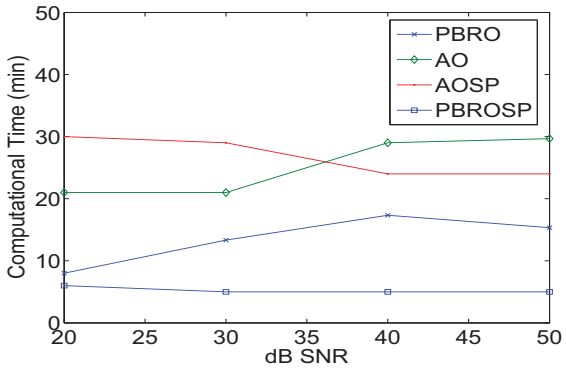

(b)

Fig. 1. This figure illustrates a comparison between the standard sequential and parallel alternating optimization algorithms, and the effect of a step-size penalization.

of interference between sequential stimuli, which in turn lowered the overall amount of information.

Finally, we tested the pOSP estimation using all five stimuli (we will refer to an experiment using all five stimuli as an "all stimuli" experiment) under different noise levels. We considered three cases: 25dB SNR with no temporal filtering, 25dB SNR with a low pass sliding window of three time-steps, and 50dB SNR with no temporal filtering. As we can observe from the results in Table I, even with high noise the pOSP can produce good estimates of the original conductive-tensor fields. Ten runs of the pOSP with differing initial fields were performed to check whether there were multiple minima. The results in Table I are from the first run; all the runs produced almost identical results.

C. Testing on a Real Data

We applied the pOSP method to a normalized data set from cardiomyocyte tissue of a newborn mouse, recorded at the Italian Institute of Technology using the high-resolution 4096-channel MEA platform of 3Brain GmbH, Switzerland.

To use the pOSP algorithm, first the optimal reaction parameters must be inferred from the data. To define the boundary conditions of the tissue, locations where the sensors had a total cumulative activity less than the threshold

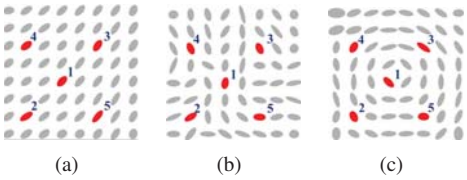

(a) (b) (c)

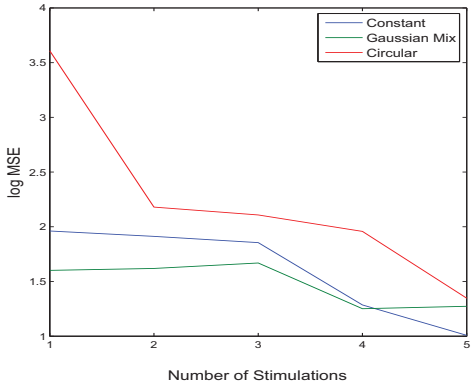

(d)

Fig. 2. Figs 2(a), 2(b), and 2(c), illustrates constant, Gaussian mix, and circular conductive fields, respectively. The stimuli positions and order are also marked. Figure 2 illustrates the effect of an increasing number of stimuli on the log mean squared error.

TABLE I

RESULTS OF "ALL STIMULI" EXPERIMENTS UNDER DIFFERENT NOISE LEVELS: I. 25 DB SNR, II. 25 DB SNR WITH TEMPORAL FILTER, AND III. 50 DB SNR.

	Original	I	II	III
Constant				
Gaussian				
Circular				

were considered to be not conductive, and hence the conductivity tensors in these locations were set to zero. We used tensor-volume constraints of $[0.3, 2]$, a spatial penalization penalty of $\mu = 10^{-12}$, and a step-size penalty $\lambda = 10^{-4}$. The conductivity tensor field was estimated using the pOSP algorithm and the measurements in the first phase, and is shown in Fig. 3(c).

Next we checked that our estimated tensor field indeed significantly improves the model prediction results compared to using a noninformative tensor field. For the null hypothesis, we calculated the one-step-ahead prediction (OSP) errors for 30 random tensor fields, and used these results to find the mean OSP error and confidence interval. In Fig.

3(d), we note the mean OSP error of random fields as "Mean Random Tensor Field", and the confidence interval, corresponding to 98%, is presented in gray. Further, we also compared the OSP errors for other noninformative tensors: an isotropic homogenous field (circles), a zero tensor field (all tensors set to zero), and a constant tensor field. While all of the noninformative tensor fields tested were within the confidence interval of the random fields, we can observe that for the first 13 ms the estimated tensor field resulted in an improvement to the OSP error which is statistically significant (3(d)). After 13 milliseconds, the OSP errors of the estimated and noninformative fields are relatively equal, and are within the confidence interval. This effect can be explained by the changes in both the spatial location of the wave and the change in dynamics, as explained above (Fig. 3(a)). These changes resulted in the estimated tensor field from the first phase of the wave becoming noninformative for the rest of the propagation.

V. Conclusion

We formulated a novel method for solving the inverse problem of inferring the conductivity structure of a biological tissue from a set of spatiotemporal measurements. We lowered the complexity of the optimization by using a single-step approximation employing a parallel alternate optimization method. This method breaks the original joint problem into a set of smaller subproblems that are solved in parallel, and avoids converging to local minima by using a step-size penalty. We analyzed the performance of our method using numerical examples of several electrical conductivity field topologies and noise levels, and discussed its application to real measurements obtained from a smooth cardiac mouse tissue slice, using data collected with the high-resolution 4096-channel MEA platform. This method main applications are in the study of extracellular domain conductivities in both muscle and nerve tissues. In the future, we will consider optimizing model parameter fitting from the data by employing more advanced learning schemes and better utilizing prior biological information. Further, we will extend the model to nonhomogeneous reaction dynamics and establish a methodology for fusing conductivity tensor field information from different post-stimulus experiments.

Acknowledgments

This work was supported in part by the McDonnell International Scholar Academy Fellowship, and also in part by a National Science found CCF-0963742.

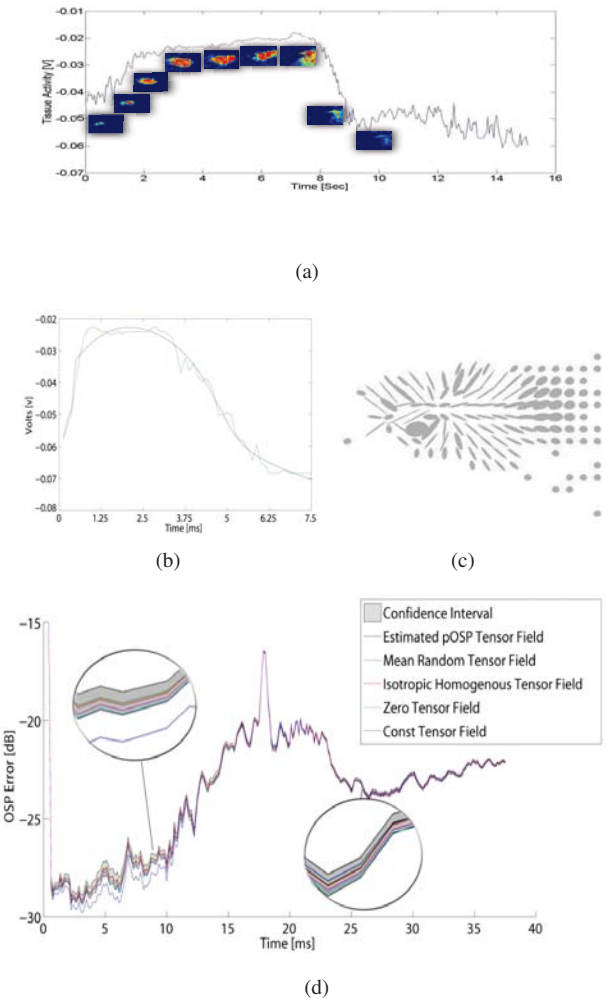

Fig. 3. Conductivity tensor field estimation of propagating waves in a slice of cardiomyocyte tissue from a newborn mouse. Fig. 3(a) illustrates the instantaneous tissue activity, and Figs. 3(b) and 3(b) illustrate the fitted reaction parameters field and estimated conductivity tensor field, respectively. Fig. 3(d) illustrates improvement of the estimated tensor field for the first 13 ms compare to other noninformative fields.

References

[1] M. L. Latash, *Neurophysiological Basis of Movement*. Human Kinetics Publishers, 2008.

[2] T. C. Pilkington, *High performance computing in biomedical research*. CRC Press, 1993.

[3] M. Bazhenov, P. Lonjers, S. Skorheim, C. Bedard, and A. Destexhe, "Non-homogeneous extracellular resistivity affects the current-source density profiles of updown state oscillations," *Philosophical Transactions of the Royal Society*, vol. 369, no. 1952, pp. 3802–3819, 2011.

[4] K. Imfeld, S. Neukom, A. Maccione, Y. Bornat, S. Martinoia, P. Farine, M. Koudelka-Hep, and L. Berdondini, "Large-scale, high-resolution data acquisition system for extracellular recording of electrophysiological activity," *Biomedical Engineering, IEEE Transactions on*, vol. 55, no. 8, pp. 2064 –2073, aug 2008.

[5] P. S. L. Rosa, H. Eswaran, H. Preissl, and A. Nehorai, "Multiscale forward electromagnetic model of uterine contractions during pregnancy," in revision for BMC Medical Physics.

[6] J. Rauch and J. Smoller, "Qualitative theory of the FitzHugh-Nagumo equations," *Advances in Mathematics*, vol. 27, pp. 12–44, 1978.

[7] T. K. Nilssen and X. C. Tai, "Parameter estimation with the augmented Lagrangian method for a parabolic equation," *journal of optimization theory and applications*, vol. 124, no. 2, pp. 435–453, 2005.

[8] A. Sitz, U. Schwarz, J. Kurths, and H. U. Voss, "Estimation of parameters and unobserved components for nonlinear systems from noisy time series," *Phys. Rev. E*, vol. 66, p. 016210, Jul 2002.

[9] A. Sitz, J. Kurths, and H. U. Voss, "Identification of nonlinear spatiotemporal systems via partitioned filtering," *Physical Review*, 2003.

[10] P. A. Valdes-Sosa, A. Roebroek, J. Daunizeau, and K. Friston, "Effective connectivity: Influence, causality and biophysical modeling," *NeuroImage*, 2011.